Blood–brain barrier changes and cell invasion differ between therapeutic immune clearance of neurotrophic virus and CNS autoimmunity

Marzena J. Fabis*†, Timothy W. Phares*‡, Rhonda B. Kean*†, Hilary Koprowski*†§, and D. Craig Hooper*†§¶

*World Health Organization Center for Neurovirology, Department of Cancer Biology, †Biotechnology Foundation Laboratories, and ¶Department of Neurological Surgery, Thomas Jefferson University, 1020 Locust Street, JAH 454, Philadelphia, PA 19107-6799

Contributed by Hilary Koprowski, August 5, 2008 (sent for review June 26, 2008)

CNS tissues are protected from circulating cells and factors by the blood–brain barrier (BBB), a specialization of the neurovasculature. Outcomes of the loss of BBB integrity and cell infiltration into CNS tissues can differ vastly. For example, elevated BBB permeability is closely associated with the development of neurological disease in experimental allergic encephalomyelitis (EAE) but not during clearance of the attenuated rabies virus CVS-F3 from the CNS tissues. To probe whether differences in the nature of BBB permeability changes may contribute to the pathogenesis of acute neuroinflammatory disease, we compared the characteristics of BBB permeability changes in mice with EAE and in mice clearing CVS-F3. BBB permeability changes are largely restricted to the cerebellum and spinal cord in both models but differ in the extent of leakage of markers of different size and in the nature of cell accumulation in the CNS tissues. The accumulation in the CNS tissues of CD4 T cells expressing mRNAs specific for IFN-γ and IL-17 is common to both, but iNOS-positive cells invade into the CNS parenchyma only in EAE. Mice that have been immunized with myelin basic protein (MBP) and infected exhibit the features of EAE. Treatment with the peroxynitrite-dependent radical scavenger urate inhibits the invasion of iNOS-positive cells into the CNS tissues and the development of clinical signs of EAE without preventing the loss of BBB integrity in immunized/infected animals. These findings indicate that BBB permeability changes can occur in the absence of neuropathology provided that cell invasion is restricted.

experimental allergic encephalomyelitis | neuroimmunology | peroxynitrite-dependent radicals | rabies virus | CNS inflammation

Contact between circulating cells and factors and CNS tissues is restricted by specializations in the neurovasculature collectively referred to as the BBB. To respond to an infection or other stimulus in the CNS tissues, immune/inflammatory cells in the circulation must be provided access across the BBB. Similarly, the proinflammatory cytokines and chemokines produced by CNS-resident cells that attract immune/inflammatory cells to the site of infection or insult must be able to reach their targets. Whether a stimulus for cell infiltration into the CNS tissues or a consequence of this process, changes in the integrity of the BBB are invariably associated with a CNS inflammatory response.

Elevations in BBB permeability to circulating markers are generally observed and investigated in the context of a pathological CNS inflammatory response. The classical example is multiple sclerosis (MS), where the leakage of gadolinium derivatives across compromised regions of the BBB is used to detect active CNS lesions (1). In experimental allergic encephalomyelitis (EAE), an animal model of autoimmune CNS inflammation that shares certain characteristics with MS, there is a clear correlation between the extent of BBB permeability to a fluid phase marker and the severity of clinical signs of disease (2–6). Similarly, the lethal outcome of Borna disease virus (BDV) infection in rats is a consequence of a neuroinflammatory response associated with the loss of BBB integrity; as long as BBB permeability changes and the CNS inflammatory response are inhibited, BDV-infected rats survive (7). Notwithstanding the general association between the loss of BBB integrity and the development of neurological disease, changes in BBB permeability are also seen in protective CNS immune responses. This is the case for infection with the attenuated strain of the neurotrophic rabies virus CVS-F3, where clearance of the virus from the mouse CNS follows increased BBB permeability and the infiltration of T and B cells into CNS tissues (8). Apart from a transient reduction in body weight that is seen when the virus is administered intranasally (i.n.), normal mice show no signs of the infection and clear the virus without incident despite its spread throughout CNS tissues and immune cell invasion (8, 9). Elevations in BBB permeability and cell invasion in animals clearing CVS-F3 are predominantly found in the cerebellum, which may limit pathological changes due to edema formation (8). This observation has led us to hypothesize that the restricted location of BBB permeability changes may be at least partly responsible for the dissociation between elevated BBB permeability and disease. Other possible contributors include limitations in the extent of the loss of BBB integrity or differences in the characteristics of the cells infiltrating the CNS tissues in CVS-F3 infection as opposed to a neuroinflammatory disease.

Understanding how therapeutic agents can be delivered across the BBB in the absence of neuropathological sequelae is paramount to the development of new strategies for the treatment of a wide variety of neurological diseases. To provide insight into how this goal may be accomplished, we have compared the location and extent of BBB permeability changes as well as the cells and mechanisms involved in triggering these changes in mice clearing CVS-F3 and mice developing the CNS inflammatory disease EAE.

Results

BBB Permeability Changes in EAE and Rabies CVS-F3 Infection Are Limited to The Cerebellum and Spinal Cord. Whereas increased neurovascular permeability to the fluid phase marker NaF is primarily seen in the cerebellum during clearance of CVS-F3 from the CNS following i.n. infection (8), the development of clinical signs of EAE has been generally associated with the loss of barrier integrity in the spinal cord (6, 10). To examine whether the location of elevated BBB permeability may be an important determinant of pathogenicity we compared BBB permeability changes in the cortex, cerebellum, and spinal cords of PLSJL mice immunized with MBP versus those infected i.n. with CVS-F3. MBP immunization caused extensive leakage of NaF from the circulation into the tissues of the spinal cord and, to a somewhat lesser extent, the

Author contributions: M.J.F., T.W.P., and D.C.H. designed research; M.J.F., T.W.P., R.B.K., and D.C.H. performed research; M.J.F., T.W.P., R.B.K., H.K., and D.C.H. analyzed data; and M.J.F., T.W.P., R.B.K., and D.C.H. wrote the paper.

The authors declare no conflict of interest.

‡Present address: Lerner Research Institute, 9500 Euclid Avenue, Cleveland, OH 44195.

§To whom correspondence may be addressed. E-mail: hilary.koprowski@jefferson.edu or douglas.hooper@jefferson.edu.

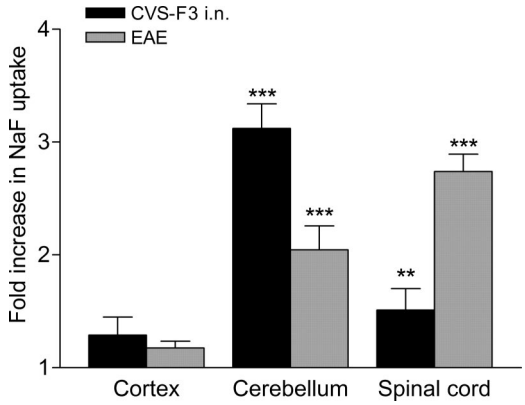

Fig. 1. Increased BBB permeability in EAE and during CVS-F3 clearance is restricted to the cerebellum and spinal cord. PLSJL mice were immunized with MBP ($n = 39$) or infected i.n. with CVS-F3 ($n = 17$) as described in *Materials and Methods*. MBP-immunized mice were scored daily for clinical signs of EAE, and BBB permeability to NaF assessed at varying disease severity (score range 3–6) as detailed in *Materials and Methods*. BBB permeability was assessed in infected mice at 7 to 8 days postinfection. BBB permeability changes are presented in as the mean ± SEM fold increase in NaF uptake in the tissues with the levels from normal mice ($n = 10$) taken as 1. Statistically significant differences in NaF uptake between immunized or infected and normal mice by the *t* test are denoted as follows: **, $P < 0.01$; ***, $P < 0.001$.

cerebellum, whereas i.n. infection with CVS-F3 caused more extensive permeability in the cerebellum than in the spinal cord (Fig. 1). Significant permeability was not detected in bulk cortex tissues, although limited areas of permeability can sometimes be visualized in the intact cortex of CVS-F3-infected mice (8).

Neurological Disease Is Associated with Elevated Neurovascular Permeability in The Spinal Cords of MBP-Immunized Mice. As shown in Fig. 2*A*, there is a linear relationship between EAE severity and the extent of NaF leakage into spinal cord tissues of PLSJL mice. In contrast, there is no correlation between disease score and the level of NaF accumulation in the cerebellum. In fact, several animals with severe EAE did not exhibit elevated BBB permeability to NaF in the cerebellum. Weight loss, the only outward manifestation after i.n. infection with CVS-F3, is associated with increased BBB permeability in the cerebellum and, to a lesser extent, the spinal cord (Fig. 2*B*).

Neurovascular Integrity Changes Permit Large Molecules to Enter CNS Tissues in EAE but Not During CVS-F3 Clearance. To determine whether the discordance in the development of neurological signs in mice clearing CVS-F3 versus those with EAE could be a result of qualitative differences in BBB permeability changes, we assessed cerebellum and spinal cord BBB permeability to circulating markers of different sizes. While markers ranging from 376 Da to 150 kDa infiltrated into the CNS tissues of mice with clinical signs of EAE, mice infected with CVS-F3 only developed significant permeability to 376 and 4000 Da markers (Fig. 3). In addition, Evans blue (EB), a dye of ≈960 Da that binds to serum proteins such as albumin (11), does not infiltrate into the CNS tissues of mice clearing CVS-F3 but accumulates in both cerebellum and spinal cord tissues of mice with EAE (Fig. 3).

IFN-γ, IL-17, and iNOS Are All Expressed in The CNS Tissues of Mice with EAE and Clearing CVS-F3. In our prior studies of CNS immunity, we have concluded that the activity of peroxynitrite-dependent radicals may contribute to BBB permeability changes in both EAE and CVS-F3 clearance (2, 12). To examine how these radicals may be produced in the two classes of CNS immune responses, we assessed tissues exhibiting enhanced vascular leakage for expression of mRNAs specific for the cytokines IFN-γ and IL-17 as well as the

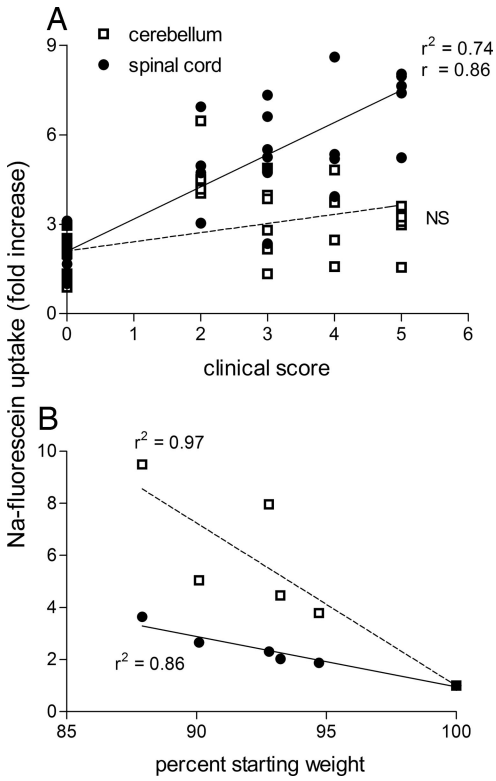

Fig. 2. Clinical severity of EAE correlates with enhanced BBB permeability in the spinal cord, whereas weight loss in CVS-F3-infected animals correlates with permeability changes in both the cerebellum and spinal cord. (*A*) Leakage of NaF into spinal cord and cerebellar tissue samples from the individual mice described in Fig. 1 is plotted against their clinical scores. (*B*) The accumulation of NaF in each tissue sample is plotted against the percentage body weight of each animal with the weight on day 0 being taken as 100%. Results of linear regression analysis (r^2) and Pearson correlation (r) are shown.

nitric oxide synthases eNOS and iNOS, because these are most likely to be associated with peroxynitrite-dependent radical formation in EAE and CVS-F3 clearance (12–16). As shown in Fig. 4*A*, the expression of IFN-γ, IL-17, and iNOS is significantly elevated in the spinal cord and cerebellum of mice with acute signs of EAE. Similar tissues from mice clearing CVS-F3 exhibit even higher levels of expression of IFN-γ, IL-17, and iNOS (Fig. 4*B*). Significantly increased expression of eNOS was limited to the spinal cord of CVS-F3-infected mice with (Fig. 4). No significant changes in any of the tested parameters were seen in the cortex (data not shown).

Administration of the Peroxynitrite-Dependent Radical Scavenger Urate Prevents BBB Permeability Changes in EAE but Not During CVS-F3 Clearance or in MBP-Immunized Mice Infected with CVS-F3. To further probe the potential contribution of peroxynitrite-dependent radicals to the mechanisms of BBB permeability changes in mice clearing CVS-F3 and mice with EAE, we compared the effects of treatment with urate, a selective scavenger of these radicals (see ref. 28) in these models. A urate treatment protocol that prevents BBB permeability changes in the cerebellum of MBP-immunized PLSJL mice fails to significantly inhibit NaF uptake into the cerebellar tissues of similar animals i.n. infected with CVS-F3 (Fig. 5). Because CVS-F3 infection induces a strong proinflammatory response in CNS-resident cells that can exacerbate the development of EAE (12), we next assessed whether CVS-F3 infection would have any impact on the effects of urate administration in MBP-immunized mice. Urate treatment inhibited the development of clinical signs of EAE in immunized/infected animals but failed to prevent the

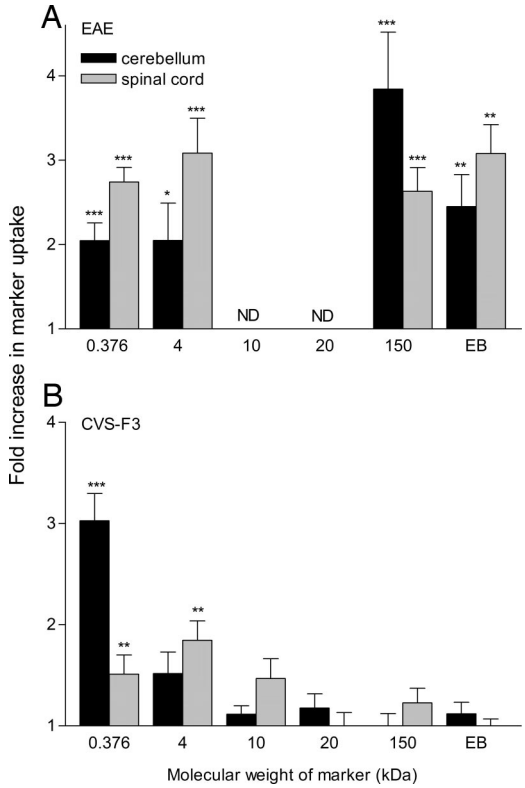

Fig. 3. The extent of BBB permeability changes to different size markers differs between mice with EAE and clearing CVS-F3. PLSJL mice were either immunized with MBP or infected i.n. with CVS-F3 RV and the extent of BBB permeability to different size markers assessed in the cerebellum and spinal cord tissues of immunized mice with disease severity scores between 3 and 5 ($n = 8–39$) or at 10 days postinfection ($n = 5–17$), as described in *Materials and Methods*. The results are expressed as the mean ± SEM fold increase in specific marker uptake in the tissues with the levels detected in tissues from normal mice taken as 1. Statistically significant differences in marker uptake between immunized or infected and normal mice, determined by the *t* test are denoted as follows: *, $P < 0.05$; **, $P < 0.01$; and ***, $P < 0.001$.

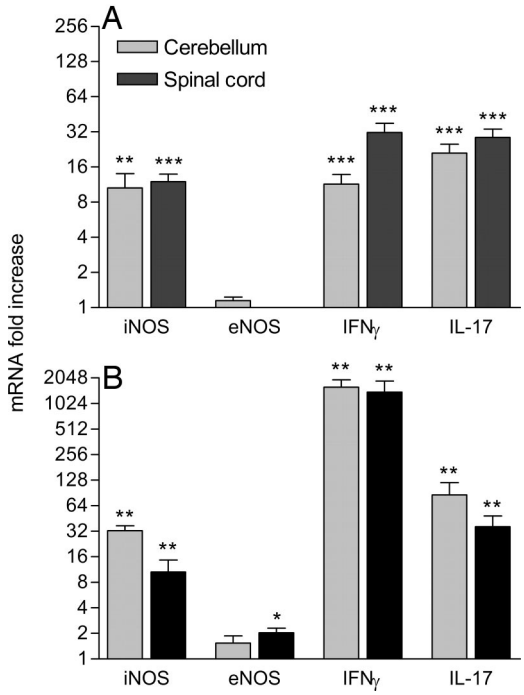

Fig. 4. Patterns of accumulation of IFN-γ, IL-17, and iNOS mRNAs are similar in the cerebellum and spinal cords of MBP-immunized (*A*) and CVS-F3-infected mice (*B*). Cerebellum and spinal cord tissues from the mice described in the legend to Fig. 3 were assessed for iNOS, eNOS, IFNγ, and IL-17 mRNA levels by real-time quantitative RT-PCR as detailed in *Materials and Methods*. Levels are presented as the mean ± SEM fold increase in copies of specific mRNA with the copies detected in normal tissues taken as 1. Expression levels significantly higher than those of similar tissues from normal mice, as determined by the Mann–Whitney test, are denoted as follows: *, $P < 0.05$; **, $P < 0.01$; and ***, $P < 0.001$.

elevated BBB permeability normally associated with the disease (Fig. 6). Leakage of 150-kDa FITC-dextran marker from the circulation into CNS tissues was reduced by ≈50%, whereas that of NaF was unchanged (Fig. 6).

The Patterns of CD4 T Cell Invasion as well as iNOS Expression and Nitrotyrosine Formation Differ Between MBP-Immunized, CVS-F3-Infected, and Immunized/Infected Mice in the Presence and Absence of Urate Treatment. To provide insight into the cell interactions at the neurovasculature that may contribute to the differences in BBB permeability changes between EAE and CVS-F3 clearance, we compared the distribution of CD4, iNOS, and the peroxynitrite-dependent radical product nitrotyrosine in sections from the cerebella of urate and saline vehicle-treated PLSJL mice immunized with MBP, infected with CVS-F3, or both immunized and infected (Fig. 7). In CVS-F3-infected mice, CD4 T cells and iNOS expression are both primarily associated with the vascular endothelium as is nitrotyrosine (Fig. 7 *D–F Upper*). There is no cell accumulation in the perivascular space and only a few CD4-positive T cells but no iNOS-positive cells nor nitrotyrosine residues are apparent in the parenchyma. Urate treatment has no discernable effect on these patterns (Fig. 7 *D–F Lower*). In contrast, CD4 T as well as iNOS-positive cells cross the vascular endothelial cells of the BBB and accumulate in the perivascular space and infiltrate into the parenchyma in saline vehicle-treated mice with EAE (Fig. 7 *G* and *H Upper*). Extensive nitrotyrosine staining is associated with the presence of iNOS-positive cells (Fig. 7*I Upper*). As previously reported (2), urate treatment of MBP-immunized mice prevents all of these changes (Fig. 7 *G–I Lower*) with the neurovasculature and cerebellar tissues appearing similar to those of normal mice (Fig. 7 *A–C*). Massive perivascular accumulation and infiltration of CD4 and iNOS-positive cells into cerebellar tissues in association with extensive parenchymal nitrotyrosine staining is seen in saline-treated mice immunized with MBP and infected with CVS-F3 (Fig. 7 *J–L Upper*). Urate treatment of infected/immunized animals prevents the appearance of these markers in both the parenchyma and perivascular space, restricting their expression to the area of the vascular endothelium (Fig. 7 *J–L Lower*).

Discussion

Whether therapeutic in the clearance of rabies CVS-F3 virus from the CNS tissues or pathological in the induction of EAE, immune cell infiltration into CNS tissues is accompanied by changes in the integrity of the BBB. When assessed by leakage of the fluid phase marker NaF from the circulation into CNS tissues, the location of BBB permeability changes is similar in PLSJL mice with EAE and those clearing CVS-F3, primarily occurring in the cerebellum and spinal cord. The absence of detectable BBB permeability changes in the cortex supports our hypothesis, initially drawn from studies of mice clearing CVS-F3 (8), that immune access to brain tissues is more tightly controlled in the cerebral cortex.

The extent of leakage of NaF from the circulation into the cerebellum and spinal cord is comparable in mice with EAE or i.n. infected with CVS-F3. However, there is clearly more extensive permeability of the BBB in the cerebellum and spinal cord to

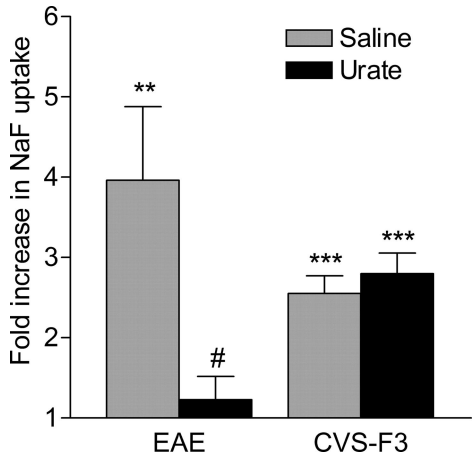

Fig. 5. Inactivation of peroxynitrite-dependent radicals prevents the loss of BBB integrity in MBP-immunized mice but has no effect on BBB permeability changes in CVS-F3 RV-infected mice. Groups of PLSJL mice (n = 5–8) were either left untreated, immunized with MBP, or infected i.n. with CVS-F3 RV and treated with 4 daily i.p. doses of 10 mg of urate or saline vehicle starting at 10 days postimmunization or 2 days postinfection. BBB permeability was assessed by measuring NaF uptake into the spinal cord tissues of MBP-immunized mice when saline vehicle-treated mice reached an average score >3 or into the cerebellum tissues of CVS-F3 RV-infected animals at 10 days postinfection. All procedures were performed as detailed in *Materials and Methods* and the results are presented as the mean ± SEM fold increase in NaF accumulation in the tissues with the levels from uninfected mice taken as 1. Statistically significant differences between the levels in experimental and normal mice, determined by the t test, are denoted as follows: **, $P < 0.01$; ***, $P < 0.001$. Significant differences in the mean levels of NaF uptake between urate- and saline-treated animals established by the t test are denoted by #, $P < 0.05$.

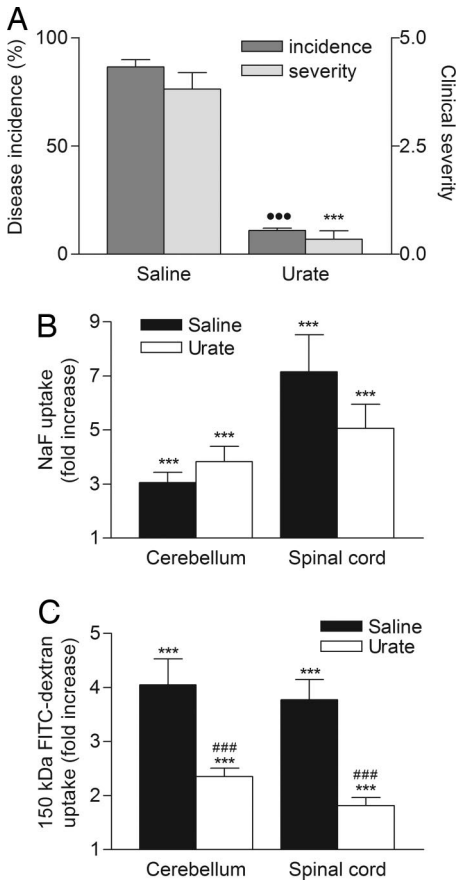

Fig. 6. Urate treatment inhibits the onset of EAE in MBP-immunized mice infected with CVS-F3 RV but does not fully protect against enhanced BBB permeability. PLSJL mice were immunized with MBP and then infected 5 days later with CVS-F3 RV. Beginning 6 h postinfection animals received 4 daily i.p. doses of either 10 mg of urate in saline (n = 26) or saline alone (n = 28). Mice were scored daily for clinical signs of EAE and the results are presented as the mean clinical score in *A*. At 12–16 days postimmunization, when the mean score of the saline controls was >3, the extent of BBB permeability changes was assessed by measuring the amount of NaF (*B*) or 150-kDa dextran-FITC (*C*) leakage into cerebellum and spinal cord tissues. All procedures were performed as detailed in *Materials and Methods*. Significant differences between urate- and saline-treated mice in incidence (●●●, $P < 0.001$ by Fishers exact test) and severity (***, $P < 0.001$ by the Mann–Whitney test) as well as significant differences in marker uptake between immunized/infected mice and normal controls (***, $P < 0.001$) and between urate- and saline-treated immunized/infected mice (###, $P < 0.001$ by the t test) are shown.

molecules from 10 to 150 kDa in EAE. The finding that 150-kDa molecules do not cross the BBB during CVS-F3 infection has implications for clearance of the virus because appreciable amounts of circulating antibodies probably do not reach infected CNS tissues. Consequently, as we have previously suggested (8), it is likely that the neutralizing antibodies required to clear the virus are produced in the CNS tissues by infiltrating B cells. Since larger molecules can cross the BBB in EAE, the association between the severity of EAE and the extent of spinal cord BBB permeability implies that there may be a causal relationship between the pathogenesis of the disease and the infiltration of large molecules into spinal cord tissues. The results of our studies of urate treatment in MBP-immunized, CVS-F3-infected mice challenge this concept. Urate selectively inactivates a radical or radicals formed by the reaction of peroxynitrite, the product of NO and superoxide, with carbon dioxide (17) and protects against the loss of BBB integrity in MBP-immunized PLSJL mice (2). Alternately, urate treatment has no impact on the elevation of BBB permeability to low molecular mass markers and only partly reduces the leakage of 150-kDa marker if MBP-immunized PLSJL mice are also infected with CVS-F3. Nevertheless, urate treatment prevents the development of clinical signs of EAE in immunized/infected mice, suggesting that the leakage of serum-borne factors into the CNS parenchyma is not solely responsible for the pathogenesis of the disease.

Our current findings are consistent with the hypothesis that the nature of cell invasion into CNS tissues bears primary responsibility for the development of clinical disease in EAE. CNS tissue levels of mRNAs specific for IFN-γ, IL-17, eNOS, and iNOS are considerably higher in CVS-F3-infected mice than in MBP-immunized mice at the peak of BBB permeability. However, the distribution of CD4 T and iNOS-positive cells is considerably different between these two models. Restricted to the region of the neurovascular endothelium in CVS-F3 infected animals, these cells accumulate in the perivascular space and invade deep into the CNS parenchyma of mice with EAE. The therapeutic effects of urate on clinical disease in MBP-immunized mice is associated with the failure of these immune/inflammatory cells to both associate with the vascular endothelium and invade CNS tissues. In the case of urate-treated, MBP-immunized mice infected with CVS-F3, CD4, and iNOS staining can be seen associated with the neurovasculature but, despite elevated BBB permeability, cells expressing these markers fail to infiltrate the CNS tissues and the animals remain healthy.

The invasion of iNOS-positive cells into the CNS tissues is associated with the activity of peroxynitrite-dependent radicals in the neural parenchyma as evidenced by the formation of nitrotyrosine. We have previously found that urate treatment of mice with ongoing EAE promotes their recovery from clinical signs of the disease (2, 18). Lesions in the spinal cord tissues of such animals still contain iNOS-positive cells but nitrotyrosine staining is considerably reduced (2). Taken together with the current findings, this finding suggests that urate-sensitive peroxynitrite-dependent radicals may have a key role in the pathogenesis of EAE in PLSJL mice.

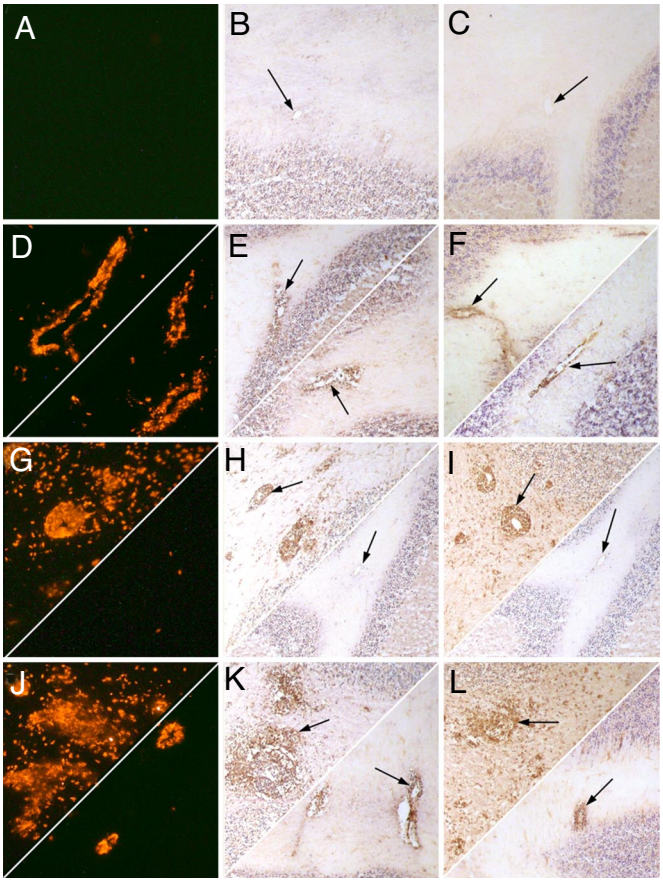

Fig. 7. The patterns of CD4 and iNOS cell accumulation as well as nitrotyrosine formation in the cerebellum differ between mice immunized with MBP, infected with CVS-F3, and both immunized and infected and treated with urate versus saline. Sections from the cerebella of normal (*A–C*), CVS-F3-infected (*D–F*), MBP-immunized (*G–I*), and MBP-immunized, CVS-F3 -infected (*J–L*) PLSJL mice treated with saline (*Upper Left*) or urate in saline (*Lower Right*) were stained for CD4 (column *A*; red), iNOS (column *B*; brown, arrowed) and nitrotyrosine (column *C*; brown, arrowed) as described in *Materials and Methods*. Photomicrographs are presented at a magnification of ≈×150.

A number of pathogenic mechanisms have been proposed for these radicals including functional changes in proteins, such as the activation of matrix metalloproteinases (19) and direct cytotoxicity for CNS-resident cells (20, 21).

We consider that the patterns of cell accumulation in the CNS tissues also provide insight into the differences in the extent of BBB permeability changes between the models studied here. The invasion of lymphocytes into CNS tissues during the clearance of CVS-F3 does not require nor cause extensive BBB leakage for large proteins. Perivascular cell accumulation is limited and the astrocyte foot processes of the glia limitans remain associated with neurovascular endothelial cells. In contrast, the invasion of CD4 T and iNOS-positive cells into CNS tissues in EAE is associated with extensive perivascular cell accumulation and clear separation between the vascular endothelial cells and the glia limitans. We speculate that the loss of the associations between the astrocyte foot processes of the glia limitans and the vascular endothelial cells is related to extensive permeability for larger molecules. A simplified illustration of the differences between these two states of elevated BBB permeability is presented in Fig. 8.

Regardless of the model or the presence of elevated serum urate levels, in all of the situations where BBB permeability became elevated in the current study, both iNOS and nitrotyrosine are detectable in the neurovasculature. This finding supports our

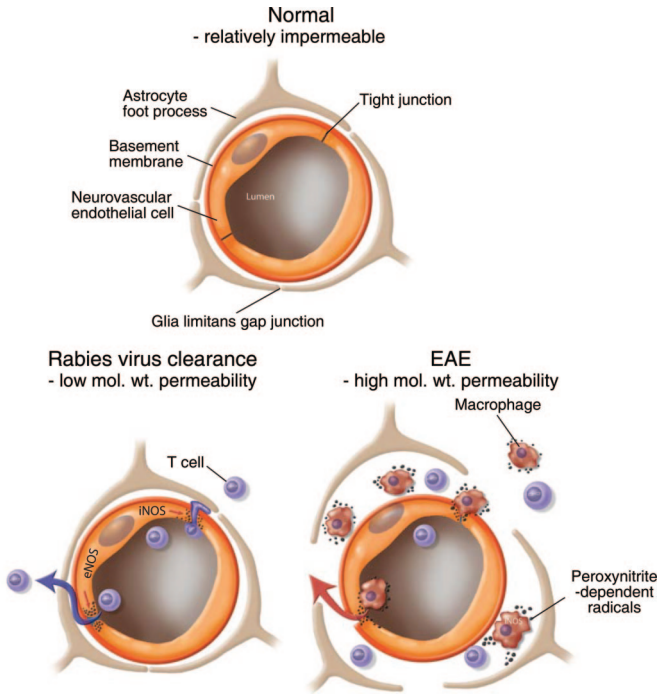

Fig. 8. Schematic representation of the changes in the relationships between endothelial cells and astrocytes of the BBB that occur in the different classes of permeability changes and CNS inflammation.

hypothesis that peroxynitrite-dependent radicals are an important immunological trigger of elevated BBB permeability (22). We speculate that there is a direct association between the capacity of urate to inhibit nitrotyrosine formation in the neurovasculature and its effects on BBB permeability. We further hypothesize that there are differences in the accessibility of urate to the sources of peroxynitrite-dependent radicals between EAE and CVS-F3 clearance. In EAE, the peroxynitrite-dependent radicals associated with the loss of BBB integrity are largely produced by iNOS-positive cells that appear in the circulation before invading CNS tissues (23). Sufficient levels of serum urate inactivate these radicals before they can cause BBB permeability changes and an associated CNS proinflammatory response (2). This outcome contrasts with CVS-F3 clearance where iNOS expression is localized in the neurovasculature and the infection induces a CNS proinflammatory independently of changes in BBB permeability. In this case, the source and targets of peroxynitrite-dependent radicals are closely approximated and urate, which does not cross the intact BBB (2), is evidently unable to inhibit nitration. A CNS proinflammatory response may also interfere with the capacity of urate to inhibit MBP-stimulated BBB permeability changes as evidenced by the inability to prevent leakage of the 150 kDa marker in MBP-immunized mice infected with CVS-F3. These findings have important implications with respect to CNS antiviral immunity in humans in demonstrating that the high serum urate levels that have evolved in humans (24), could protect against CNS autoimmunity without interfering with mechanisms involved in virus clearance.

Based on the current findings we conclude that neuropathological changes are avoided in clearing neurotrophic virus by restricting BBB permeability changes in the cortex, limiting neurovascular permeability in the cerebellum and spinal cord to small molecules, and by preventing iNOS-positive cell invasion into the CNS parenchyma. Providing that these criteria are met, the CD4, CD8, and B cells that are associated with the clearance of CVS-F3 can be delivered to the CNS tissues without pathological sequelae.

Materials and Methods

Mice, Immunization, Infection, and Treatment. Female, 8–10-week-old PLSJL mice purchased from The Jackson Laboratory and maintained under pathogen-free conditions were used in this study. The EAE induction protocol consisted of s.c. immunization with MBP in Freund's complete adjuvant with Pertussis toxin i.p. on days 0 and 2, as previously described (14). The animals were scored for clinical signs of EAE daily with: 0, normal mouse; 1, tail weakness; 2, tail paralysis; 3, tail paralysis plus hind limb weakness; 4, tail paralysis plus partial hind limb paralysis; 5, complete hind limb paralysis; 6, hind and fore limb paralysis; and 7, moribund/dead. Infection with CVS-F3 was i.n., with 10^5 focus forming units as previously described (12). Mice were treated with urate (Sigma and Aldrich) as a 10-mg suspension in 100 μl of saline i.p. four times daily beginning at day 5 p.i. as detailed previously (18). Controls received a similar regimen of saline vehicle. All procedures were conducted in accordance with federal guidelines under animal protocols approved by the Thomas Jefferson University Institutional Animal Care and Use Committee.

Determination of BBB Permeability. BBB permeability was assessed by using previously described techniques (2, 25) and the following markers diluted in PBS: sodium-fluorescein (NaF, 376 Da; 100 μl of 100 mg/ml i.p.); fluorescein-dextran (FITC-dextran) of molecular mass 4,000 Da (200 μl of 250 mg/ml i.v.); 10,000 Da (200 μl of 100 mg/ml i.v.); 20,000 Da (200 μl of 200 mg/ml i.v.); 150,000 Da (200 μl of 37.5 mg/ml i.v.); or EB (200 μl of 20 mg/ml i.v.) (all obtained from Sigma). EB has a nominal molecular mass of 960 Da but is known to bind to serum proteins such as albumin (11). The markers were allowed to circulate in the mice for 10 min with the exception of FITC-dextran-150,000, which circulated for 4 h before transcardial perfusion, sample collection, and preparation. CNS tissues were homogenized in PBS, centrifuged, and the supernatants clarified by using 7.5% trichloroacetic acid. For FITC markers, NaOH was added to a final concentration of 1 M and fluorescence at 485-nm excitation and 530-nm emission was determined by using a Cytofluor II fluorimeter (PerSeptive Biosystems). EB levels were assessed by absorbance at 620 nm by using a NanoDrop-1000 spectrophotometer (NanoDrop Technologies). Marker content was calculated by using standards and uptake from the circulation into CNS tissue calculated as (μg marker in CNS tissue/mg protein)/(μg marker in sera/μl blood) to normalize values for blood levels. Data are expressed as a fold increase in the amount of marker in the tissues by comparison with the values obtained for tissues from similarly assessed normal mice.

Real-Time Quantitative RT-PCR. Isolation of mRNA and quantification of specific mRNA levels were performed by real-time quantitative RT-PCR by using previously described primers, probes, and methodologies (8, 26–28) and a BioRad iCycler iQ real-time detection system with the exception of IL-17 mRNA, where a FAM-labeled probe (ACCCTGGACTCTCCACCGCAATGA) was used with published primers. Data were calculated based on the threshold cycle (Ct), the PCR cycle at which the fluorescent signal becomes higher than that of the background (cycles 2–10) plus 10 $\times$ SD. Synthetic cDNA standards were used to determine copy numbers. Data are expressed as the fold increase in mRNA copy numbers in test tissues over levels in control tissue samples from naive mice, with all values normalized to the L13 mRNA content of each sample.

Immunohistochemistry. Immunohistochemical analysis was performed as previously described (2, 12) by using phycoerythrin (PE)-conjugated monoclonal anti-CD4, (BD PharMingen), rabbit polyclonal anti-NOS2 (Santa Cruz Biotechnology), and rabbit polyclonal anti-nitrotyrosine (Upstate Biotechnology). Staining with the polyclonal antibodies was detected by using the peroxidase antiperoxidase method (Sternberger Monoclonals, Inc.) and 3′3-diaminobenzidine (brown) substrate. For the latter, sections were counterstained with Harris' hematoxylin (blue nuclear stain). Photographs were taken with a Nikon digital camera on an Olympus microscope and are reproduced at the final magnification noted in the figure legends.

Statistical Analyses. Results are expressed as the mean $\pm$ SEM for groups of 5–39 mice. Evaluation of the significance of differences between groups was performed by using the unpaired *t* test or the Mann–Whitney test for nonparametric results. Fisher's exact test was used for contingency analysis, whereas linear regression and the Pearson *r* test were used to assess relationships between two parameters. Graphs were plotted and statistics assessed by using Graphpad Prism 3.0 (GraphPad Software, Inc.).

ACKNOWLEDGMENTS. We thank Drs. Mikhail Prosniak and Anirban Roy for helpful discussions and Paul Schiffmacher for the design of Fig. 8. This work was supported in part by National Institutes of Health Grants AI-077033 and AI-060005 and by a grant to the Biotechnology Foundation Inc. from the Commonwealth of Pennsylvania.

1. Grossman RI, Gonzalez-Scarano F, Atlas SW, Galetta S, Silberberg DH (1986) Multiple sclerosis: Gadolinium enhancement in MR imaging. *Radiology* 16:721–725.
2. Hooper DC, *et al.* (2000) Uric acid, a peroxynitrite scavenger, inhibits CNS inflammation, blood-CNS barrier permeability, and tissue damage in a mouse model of multiple sclerosis. *FASEB J* 14:691–698.
3. Kean RB, Spitsin SV, Mikheeva T, Scott GS, Hooper DC (2000) The peroxynitrite scavenger uric acid prevents inflammatory cell invasion into the central nervous system in experimental allergic encephalomyelitis through maintenance of blood-central nervous system barrier integrity. *J Immunol* 165:6511–6518.
4. Paul C, Bolton C (2002) Modulation of blood–brain barrier dysfunction and neurological deficits during acute experimental allergic encephalomyelitis by the N-methyl-D-aspartate receptor antagonist memantine. *J Pharmacol Exp Ther* 302:50–57.
5. Floris S, *et al.* (2004) Blood–brain barrier permeability and monocyte infiltration in experimental allergic encephalomyelitis: A quantitative MRI study. *Brain* 127:616–627.
6. Fabis MJ, Scott GS, Kean RB, Koprowski H, Hooper DC (2007) Loss of blood–brain barrier integrity in the spinal cord is common to experimental allergic encephalomyelitis in knockout mouse models. *Proc Natl Acad Sci USA* 104:5656–5661.
7. Hooper DC, *et al.* (2001) The central nervous system inflammatory response to neurotrophic virus infection is peroxynitrite dependent. *J Immunol* 167:3470–3477.
8. Phares TW, Kean RB, Mikheeva T, Hooper DC (2006) Regional differences in blood–brain barrier permeability changes and inflammation in the apathogenic clearance of virus from the central nervous system. *J Immunol* 176:7666–7675.
9. Hooper DC, *et al.* (1998) Collaboration of antibody and inflammation in clearance of rabies virus from the central nervous system. *J Virol* 72:3711–3719.
10. Juhler M, *et al.* (1984) Blood–brain and blood-spinal cord barrier permeability during the course of experimental allergic encephalomyelitis in the rat. *Brain Res* 302:347–355.
11. Patterson CE, Rhoades RA, Garcia JGN (1992) Evans blue dye as a marker of albumin clearance in cultured endothelial monolayer and isolated lung. *J Appl Physiol* 72:865–873.
12. Phares TW, Fabis MJ, Brimer CM, Kean RB, Hooper DC (2007) A peroxynitrite-dependent pathway is responsible for blood–brain barrier permeability changes during a central nervous system inflammatory response: TNF-α is neither necessary nor sufficient. *J Immunol* 178:7334–7343.
13. Cross AW, Manning PT, Stern MK, Misko TP (1997) Evidence for the production of peroxynitrite in inflammatory CNS demyelination. *J Neuroimmunol* 80:121–130.
14. Hooper DC, *et al.* (1997) Prevention of experimental allergic encephalomyelitis by targeting nitric oxide and peroxynitrite: Implications for the treatment of multiple sclerosis. *Proc Natl Acad Sci USA* 94:2528–2533.
15. Miljkovic D, Trajkovic V (2004) Inducible nitric oxide synthase activation by interleukin-17. *Cytokine Growth Factor Rev* 15:21–32.
16. Langrish CL, *et al.* (2005) IL-23 drives a pathogenic T cell population that induces autoimmune inflammation *J Exp Med* 201:233–240.
17. Squadrito GL, *et al.* (2000) Reaction of uric acid with peroxynitrite and implications for the mechanism of neuroprotection by uric acid. *Arch Biochem Biophys* 376:333–337.
18. Hooper DC, *et al.* (1998) Uric acid, a natural scavenger of peroxynitrite, in experimental allergic encephalomyelitis and multiple sclerosis. *Proc Natl Acad Sci USA* 95:675–680.
19. Rajagopalan S *et al.* (1996) Reactive oxygen species produced by macrophage-derived foam cells regulate the activity of vascular matrix metalloproteinases in vitro. Implications for artherosclerotic plaque stability. *J Clin Invest* 98:2572–2579.
20. Trackey JL, Uliasz TF, Hewitt SJ (2001) SIN-1-induced cytotoxicity in mixed cortical cell culture: Peroxynitrite-dependent and -independent induction of excitotoxic cell death. *J Neurochem* 79:445–455.
21. Scott GS, Virág L, Szabó C, Hooper DC (2003) Peroxynitrite-induced oligodendrocytes-toxicity is not dependent on poly(ADP-ribose) polymerase activity. *Glia* 41:105–116.
22. Scott GS, Hooper DC (2001) The role of uric acid in protection against peroxynitrite-mediated pathology. *Med Hypotheses* 56:95–100.
23. Spitsin SV, Scott GS, Kean RB, Mikheeva T, Hooper DC (2000) Protection of myelin basic protein immunized mice from free-radical mediated inflammatory cell invasion of the central nervous system by the natural peroxynitrite scavenger uric acid. *Neurosci Lett* 292:137–141.
24. Varela-Eschavarria A, Montes de Oca-Luna R, Barrera-Saldana HA (1988) Uricase protein sequences: Conserved during hominid evolution but absent in humans. *FASEB J* 2:3092–3096.
25. Saria A, Lundberg JM (1983) Evans blue fluorescence: Quantitative and morphological evaluation of vascular permeability in animal tissues. *J Neurosci Methods* 8:41–49.
26. Hsu HC, *et al.* (2008) Interleukin 17-producing T helper cells and interleukin 17 orchestrate autoreactive germinal center development in autoimmune BXD2 mice. *Nat Immunol* 9:166–175.
27. Shih SC, Smith LE (2005) Quantitative multi-gene transcriptional profiling using real-time PCR with a master template. *Exp Mol Pathol* 79:14–22.
28. Scott GS, *et al.* (2004) ICAM-1 upregulation in the spinal cords of PLSJL mice with experimental allergic encephalomyelitis is dependent upon TNF-α production triggered by the loss of blood-brain barrier integrity. *J Neuroimmunol* 155:32–42.